A&A 538, A119 (2012)
DOI: 10.1051/0004-6361/201117072

Astronomy & Astrophysics

Microwave and submillimeter spectroscopy and first ISM detection of ^{18}O-methyl formate⋆

B. Tercero[1], L. Margulès[2], M. Carvajal[3], R. A. Motiyenko[2], T. R. Huet[2], E. A. Alekseev[4], I. Kleiner[5], J. C. Guillemin[6], H. Møllendal[7], and J. Cernicharo[1]

[1] Centro de Astrobiología (CSIC-INTA). Laboratory of Molecular Astrophysics. Department of Astrophysics. Ctra de Ajalvir, Km 4, 28850 Torrejón de Ardoz, Madrid, Spain
[2] Laboratoire de Physique des Lasers, Atomes, et Molécules, UMR CNRS 8523, Université de Lille I, 59655 Villeneuve d'Ascq Cedex, France
e-mail: laurent.margules@univ-lille1.fr
[3] Departamento de Física Aplicada, Facultad de Ciencias Experimentales, Universidad de Huelva, 21071 Huelva, Spain
[4] Institute of Radio Astronomy of NASU, Chervonopraporna Str., 4, 61002 Kharkov, Ukraine
[5] Laboratoire Interuniversitaire des Systèmes Atmosphériques, UMR CNRS/IPSL 7583, Université Paris 7 et Université Paris Est, 61 Av. Charles de Gaulle, 94010 Créteil Cedex, France
[6] Sciences Chimiques de Rennes, École Nationale Supérieure de Chimie de Rennes, CNRS, UMR 6226, Avenue du Général Leclerc, CS 50837, 35708 Rennes Cedex 7, France
[7] Centre for Theoretical and Computational Chemistry (CTCC), Department of Chemistry, University of Oslo, PO Box 1033, Blindern, 0315 Oslo, Norway

Received 13 April 2011 / Accepted 3 October 2011

ABSTRACT

Context. Astronomical survey of interstellar molecular clouds needs a previous analysis of the spectra in the microwave and sub-mm energy range to be able to identify them. We obtained very accurate spectroscopic constants in a comprehensive laboratory analysis of rotational spectra. These constants can be used to predict transition frequencies that were not measured in the laboratory very precisely.
Aims. We present an experimental study and a theoretical analysis of two ^{18}O-methyl formate isotopologues, which were subsequently detected for the first time in Orion KL.
Methods. The experimental spectra of both methyl formate isotopologues recorded in the microwave and sub-mm range from 1 to 660 GHz. Both spectra were analysed by using the rho-axis method (RAM) which takes into account the CH_3 internal rotation.
Results. We obtained spectroscopic constants of both ^{18}O- methyl formate with high accuracy. Thousands of transitions were assigned and others predicted, which allowed us to detect both species in the IRAM 30 m line survey of Orion KL.

Key words. astrochemistry – ISM: molecules – submillimeter: ISM – line: identification – astronomical databases: miscellaneous – ISM: individual objects: Orion KL

1. Introduction

Complex organic molecules are relatively heavy and therefore have their maximum absorptions in the millimeter domain at about 300 GHz. But the most abundant compounds, like methyl formate, can be detected in the ISM up to 900 GHz (Comito et al. 2005). Since the first detection of this compound in 1975 (Brown et al. 1975; Churchwell et al. 1975), nearly one thousand lines were detected in the ground torsional state $v_t = 0$ (Lovas 2004) in star-forming regions (Sakai al. 2007, and references therein). The column density depends on the object, it goes from 8.8×10^{15} in NGC 2264 MMS 3 (Sakai al. 2007) to 3.4×10^{17} cm^{-2} in G19.61-0.23 (Remijan et al. 2004). Because of this fairly high column density, some lines from the first torsional state were also detected in Orion KL (Kobayashi et al. 2007) and in W51e2 (Demyk et al. 2008).

The spectra of the complex organic molecules are dense, and when a compound is abundant, for example methyl formate, one can detect the lines from the lower energy excited states, but also those from isotopic species. They can only be unambiguously detected if laboratory measurements and theoretical modelling are performed. Accurate line-by-line predictions for the positions and intensities were obtained for this purpose. Laboratory spectroscopic studies are therefore very important to be able to satisfactorily treat the spectra that are or will be obtained with submillimeter wave facilities *Herschel*, ALMA, and SOFIA.

Consequently, we decided to study the entire mono-isotopic species of methyl formate (Willaert et al. 2006; Carvajal et al. 2007, 2009, 2010; Margulès et al. 2009a, 2010; Demaison et al. 2010). These studies allowed the detection of more than 400 lines of both ^{13}C isotopologues and 100 lines of $DCOOCH_3$ in Orion KL.

The first laboratory measurements of the rotational spectra of methyl formate were made by Curl (1959). But the first general analysis of the internal rotation splitting (A and E) was made in 1999 (Oesterling et al. 1999). A more complete summary of the

⋆ Full Tables A.1 et A.2 are available at the CDS via anonymous ftp to cdsarc.u-strasbg.fr (130.79.128.5) or via http://cdsarc.u-strasbg.fr/viz-bin/qcat?J/A+A/538/A119

spectroscopic history can be found in Carvajal et al. (2009). The only measurements of the ^{18}O isotopologues, available are those made in the centimeter-wave range by Curl (1959).

A few of the ^{18}O species have been detected up to now. The only isotopic species detected so far in SgrB2 are C^{18}O, ^{13}C^{18}O, HC^{18}O^{+}, CH$_3$^{18}OH, S^{18}O, and SO^{18}O (Belloche, priv. comm.), besides ^{28}Si^{18}O maser lines in Orion KL. Studying these is important for two main reasons: first, they give information about the isotopic ratio, as in the case of the detections of ^{18}OH (Morino et al. 1995), HC^{18}O^{+} (Guélin et al. 1979), or H$_2$^{18}O (Neufeld et al. 2000). The ^{18}O species were also useful to determine the isotopic ratio of ^{12}C-^{13}C in the case of CO (Langer et al. 1990). The second reason is that the ISM spectra should be cleaned of the lines from "weed's" isotopic species to detect new species.

2. Experiments

2.1. Lille – FTMW spectrometer

The 1–20 GHz spectra were observed using the new molecular beam Fourier transform microwave spectrometer of Lille. The basic principles and technical details remain unchanged (Kassi et al. 2000). The main improvement of the new spectrometer consists of two new mirrors (diameter of 0.7 m compared to 0.4 m previously) to improve the signal-to-noise ratio at low frequencies (diffraction losses). Signals were recorded in the 4–18 GHz spectral region. Methyl formate vapors at a pressure of 20 mbars were mixed with neon carrier gas at a backing pressure of 1.5 bar. The mixture was introduced into a Fabry-Perot cavity at a repetition rate of 1.5 Hz. Molecules were polarized within the supersonic expansion by a 2 μs pulse and the free induction decay signal was detected and digitized at a repetition rate of 120 MHz. After transformation of the time domain signal into the frequency domain, molecular lines were observed as Doppler doublets, with a signal point every 0.92 kHz, resulting from the average of about 100 coded signals. Transition frequency was measured as an average of the two Doppler components and for most of the lines the uncertainty of the measurements is estimated to be less than 2 kHz.

2.2. Oslo – Stark centimeter wave spectrometer

The spectra of HC^{18}OOCH$_3$ and of HCO^{18}OCH$_3$ were recorded in the 7–80 GHz spectral region using the Stark-modulated microwave spectrometer of the University of Oslo. Details of the construction and operation of this spectrometer have been given elsewhere (Møllendal et al. 2005, 2006). The spectrum was taken at room temperature, or at roughly –20 °C at a pressure of approximately 10 Pa, employing a Stark field strength of about 1100 V/cm. The frequency of individual transitions has an estimated accuracy of ≈0.15 MHz

2.3. Lille – Submillimeter wave (SMM) spectrometer

The submillimeter-wave measurements (150–660 GHz) were performed using the Lille spectrometer (Motiyenko et al. 2010). In the frequency ranges: 150–322 and 400–533 GHz the solid state sources were used. The frequency of the Agilent synthesizer (12.5–17.5 GHz) was first multiplied by six and amplified by a Spacek active sextupler, providing the output power of +15 dBm in the *W*-band range (75–110 GHz). This power is high enough to use passive Schottky multipliers (X2, X3, X5) from Virginia Diodes Inc. in the next stage of the frequency multiplication chain.

In the frequency range from 580 to 660 GHz our new fast-scan spectrometer was applied. In general this is a usual absorption spectrometer. As a radiation source we applied the Istok backward wave oscillator (BWO). It was phase-locked to a harmonic of Agilent E8257D synthesizer which provided in our design large-step (~100 MHz) frequency control. A high-resolution fast frequency scan provided by a direct digital synthesizer, which is used as a reference source of BWO's PLL (phase-locked loop). This solution allows us to reach a very high speed of spectra records of up to 100 GHz per hour. As a detector we used an InSb liquid He-cooled bolometer from QMC Instruments Ltd. To improve the sensitivity of the spectrometer, the sources were frequency-modulated at 10 kHz. The absorption cell was a stainless-steel tube (6 cm diameter, 220 cm long). The sample pressure during measurements was about 2.5 Pa and the linewidth was limited by Doppler broadening. The measurement accuracy for isolated line is estimated to be better than 30 kHz. However, if the lines were blended or had a poor signal-to-noise ratio they were given a weight of 100 or even 200 kHz.

2.4. Synthesis of ^{18}O-formic acid, methyl ester

Material. Formic acid, methanol and sulfuric acid (reagent grade, 95–98%) were purchased from Aldrich. ^{18}O-methanol and ^{18}O$_2$-formic acid, sodium salt were purchased from the Eurisotop Company.

H$_3$COC(^{18}O)H. In a flask were introduced ^{18}O$_2$-formic acid, sodium salt (0.72 g, 10 mmol) and methanol (0.48 g, 15 mmol). The solution was cooled to about −80 °C and we added sulfuric acid (1.0 g, 10 mmol). The mixture was then cooled in a liquid nitrogen bath and evacuated (0.1 mbar). The stopcock was closed and the solution was heated up to 40 °C and stirred overnight at this temperature. The cell was then adapted to a vacuum line equipped with two traps. The solution was distilled and higher boiling compounds were trapped in the first trap immersed in a bath cooled at –70 °C and the methyl formate H$_3$COC(^{18}O)H (0.57 g, 9.2 mmol) was condensed in the second trap immersed in a liquid nitrogen bath (−196 °C). Yield: 92% but the methanol was quite difficult to remove completely and only 0.4 g of the pure product was isolated after a second trap-to-trap distillation with a first trap cooled at –90 °C (with another sample containing about 20% of methanol).

H$_3$C^{18}OC(O)H. The synthesis reported for the ^{13}C derivative (Carvajal et al. 2009) was used starting from formic acid (2.0 g, 43 mmol) and ^{18}O-methanol (1.0 g, 29 mmol). Yield: 97% (1.7 g, 28 mmol).

^{1}H and ^{13}C NMR spectra of H$_3$C^{18}OC(O)H and H$_3$COC(^{18}O)H are identical to those of the ^{16}O derivative.

3. Theoretical model

The theoretical model and the so-called RAM method (rho-axis method) used for the present spectral analyses and fits of the HC^{18}OOCH$_3$ and HCO^{18}OCH$_3$ species have also been used previously for a number of molecules containing an internal methyl rotor (see for example Ilyushin et al. 2003, 2008) and in particular for the normal species of the cis-methyl formate (Carvajal et al. 2007; Ilyushin et al. 2009), for the H^{13}COOCH$_3$ and HCOO^{13}CH$_3$ species (Carvajal et al. 2009, 2010) and for DCOOCH$_3$ (Margulès et al. 2010). The RAM Hamiltonian used in the present study is based on previous works (Kirtman 1962; Lees & Baker 1968; Herbst et al. 1984). This method takes

its name from the choice of the axis system that allows one to minimize the coupling between internal rotation and global rotation in the Hamiltonian, at least to zeroth order. Because this method has been presented in great details in the literature (Lin & Swalen 1959; Hougen et al. 1994; Kleiner 2010), we will not describe it here.

The principal advantage of the RAM global approach used in our code BELGI, which is publicly available[1], is its general approach that simultaneously takes into account the A- and E-symmetry species in our fit. All the torsional levels that originated from one given vibrational state and the interactions within those rotation-torsion energy levels are also included in the rotation-torsion Hamiltonian matrix elements. The various rotational, torsional and coupling terms between rotation and torsion that we used for the fit of the HC^{18}OOCH$_3$ and of HCO^{18}OCH$_3$ species were defined previously for the normal methyl formate species (Carvajal et al. 2007). The labelling scheme of the energy levels and transitions used for methyl formate was also described in the same reference, as was the connection with the more traditional J_{K_a,K_c} labelling.

The HC^{18}OOCH$_3$ and HCO^{18}OCH$_3$ species share a number of spectroscopic characteristics with the other isotopologues of the cis-methyl formate molecule that are summarized in Demaison et al. (2010). The potential that hinders the internal rotation has an intermediate height, V_3 = 391.569 (6) cm^{-1} and 391.356 (4) cm^{-1} for HC^{18}OOCH$_3$ and HCO^{18}OCH$_3$, respectively; thus, it produces fairly large splittings of the rotational transitions even in the ground torsional state. Its A rotational constant is fairly small (about 0.56 cm^{-1}), which permits the measurement of many transitions, including high-J transitions ($J \leq 80$). The different isotopologues of methyl formate are all fairly asymmetric near-prolate rotors ($\kappa \sim -0.78$) and this leads to the observation of a clustering of lines with the same K_c quantum number at high J and low K_a. Finally the density of the ^{18}O-methyl formate species spectrum is increased, like the case of the other isotopologues of methyl formate, by the existence of several low-lying vibrations (for the H^{12}COO^{12}CH$_3$ molecule the torsion mode is around 130 cm^{-1}, the COC bend at 318 cm^{-1}, and an out-of-plane C-O torsion mode at 332 cm^{-1}) (Chao et al. 1986). But like the other isotopologues of methyl formate we studied, no perturbation was observed in the ground state v_t = 0 data, and this was assumed in the present fit of the ^{18}O species.

4. Assignments and fit

We started the present analysis by including transitions corresponding to low values of the rotational quantum number J in the fit, floating the lower order terms, i.e. the rotational parameters A, B, C and D_{ab} used in the RAM non principal axis system, the potential barrier V_3 and ρ, the coupling term between the internal rotation angular momentum and the global rotation angular momentum. The internal rotation constant F was kept fixed to its value determined in a fit of the ground and first torsional states v_t = 0 and 1 of the normal species of methyl formate (Carvajal et al. 2007). After fitting transitions corresponding to low J values, we gradually included transitions with higher J values.

[1] The source code for the fit, an example of input data file and a readme file are available at the web site (http://www.ifpan.edu.pl/~kisiel/introt/introt.htm#belgi) managed by Dr. Zbigniew Kisiel. Extended versions of the code made to fit transitions with higher J and K are also available the authors (I. Kleiner and M.C.).

For the HCO^{18}OCH$_3$ species, a total of 4430 A and E type transitions belonging to the ground torsional state were fitted using 31 parameters (floating 30 parameters and fixing parameter F) with a unitless standard deviation of 0.60 (47.8 kHz). The spectral ranges covered by our laboratory analysis were the following: 1–19 GHz (FTMW Lille spectrometer), 7-80 GHz (Oslo Stark spectrometer), 150–322 GHz, 400–533 GHz and 583–650 GHz (Lille SMM-spectrometer). The maximum values of J and K analyzed were 62 and 30 respectively. In the dataset, the 30 transition lines measured with the FTMW were weighted 3 kHz, the 4148 unblended transitions measured by the millimeter spectrometer at Lille were weighted 30 or 50 kHz depending on the broadening of the lines, 4 blended transitions from the same spectrometer were weighted 100 kHz and the 248 transitions measured in Oslo were weighted 150 kHz.

The fit included 3258 lines for the HC^{18}OOCH$_3$ species, using 30 parameters (floating 29 parameters and again fixing the internal rotation parameter F). The unitless standard deviation for this other ^{18}O species of methyl formate is 0.82 (44.8 kHz). The same spectral ranges as for the other ^{18}O species were covered, and the weights distribution in the dataset was similar. Eleven lines measured with the FTMW spectrometer were weighted 3 kHz. Some 262 and 2628 unblended transitions measured very precisely by the millimeter spectrometer at Lille were weighted 30 or 50 kHz depending on the line broadening, 179 blended transitions from the same spectrometer were weighted 100 kHz, and 137 transitions measured in Oslo were weighted 150 kHz. Some 3 and 38 blended transitions measured in Oslo and Lille respectively were weighted 200 kHz. Tables 1 and 2 show the quality of the fit for the HCO^{18}OCH$_3$ and HC^{18}OOCH$_3$ species, respectively, with the root-mean-square deviations for the transitions according to their measurement uncertainty.

The dataset corresponding to the A-symmetry and to the E-symmetry for both ^{18}O-HCOOCH$_3$ species, that were simultaneously taken into account in the theoretical model, fit with similar root-mean-square deviations of 51 kHz and 44 kHz for HCO^{18}OCH$_3$, and 48 kHz and 41 kHz for HC^{18}OOCH$_3$, showing the quality of the fit. The unitless standard deviations obtained for the HCO^{18}OCH$_3$ and HC^{18}OOCH$_3$ species are 0.60 and 0.82, respectively, similar to those obtained for the other isotopologues of methyl formate (Ilyushin et al. 2009; Carvajal et al. 2009; Margulès et al. 2009a; Carvajal et al. 2010). Table 3 compares the results of the fits using the code BELGI for the various isotopologues of methyl formate, using the same RAM method.

Table 3 gives the values of the internal rotation parameters (V_3, F and the reduced height $s = 4V_3/9F$ and ρ), the angle θ_{RAM} between the RAM a axis and the principal axis, the angle $<(i, a)$ between the direction of the methyl group and the principal a axis, the maximum values of J_{max}, K_{max}, v_{tmax} reached in the analysis, the number of lines included in the fit, the number of floated parameters, and the unitless standard deviations. One comment should be made on the internal rotation constant F and barrier height V_3 values appearing in Table 3. As already mentioned in Carvajal et al. (2009), an analysis of rotational transitions belonging to the excited torsional states have not been performed for any of the isotopologues of methyl formate (except for the normal species H^{12}COO^{12}CH$_3$ and H^{13}COO^{12}CH$_3$ for which we recently fitted rotational lines belonging to v_t = 1 Carvajal et al. 2010). The two torsion parameters V_3 (the height of the barrier) and F (the internal rotation parameter) are therefore highly correlated in this case and cannot be fitted simultaneously. The value of the F parameter of HCOO^{13}CH$_3$ species

Table 1. Root-mean-square (rms) deviations from the global fit[a] of transitions involving $v_t = 0$ torsional energy levels of $HCO^{18}OCH_3$ methyl formate.

Number of parameters				30 (+1fixed)	
Number of lines				4430	
rms of the 4430 MW $v_t = 0$–0 lines				0.0478 MHz	
rms of the 2256 A symmetry lines				0.051 MHz	
rms of the 2174 E symmetry lines				0.044 MHz	
Source[b]	Range[c] (GHz)	v_t, J_{max}, K_{max}[d]	Number of lines[e]	Uncertainties[f] (MHz)	rms[g] (MHz)
FTMW-LILLE	1–20	0, 7, 2	30	0.003	0.0024
SMM-LILLE[h]	150–660	0, 62, 30	4148	0.030–0.050	0.0254
SMM-LILLE[h]	150–660	0, 25, 6	4	0.100	0.0769
OSLO	7–80	0, 36, 9	248	0.150	0.1729

Notes. [(a)] Parameter values are given in Table 4. The observed minus calculated residuals are given in the supplementary Table S1. [(b)] Sources of data: FTMW-LILLE, SMM-LILLE and OSLO data comes from present work, see experimental section. [(c)] Range containing the measurements in a given row. [(d)] v_t state and maximum J and K_a for each group of measurements. [(e)] Number of MW lines in each uncertainty group. [(f)] One-sigma standard uncertainty in MHz used in the fit. [(g)] Root-mean-square deviation in MHz for each group. [(h)] The SMM-LILLE spectrometer spectral ranges for these measurements are: 150–322 GHz, 400–533 GHz and 583–660 GHz.

Table 2. Root-mean-square (rms) deviations from the global fit[a] of transitions involving $v_t = 0$ torsional energy levels of $HC^{18}OOCH_3$ methyl formate.

Number of parameters				29 (+1fixed)	
Number of lines				3258	
rms of the 3258 MW $v_t = 0$–0 lines				0.0448 MHz	
rms of the 1720 A symmetry lines				0.048 MHz	
rms of the 1538 E symmetry lines				0.041 MHz	
Source[b]	Range[c] (GHz)	v_t, J_{max}, K_{max}[d]	Number of lines[e]	Uncertainties[f] (MHz)	rms[g] (MHz)
FTMW-LILLE	1–20	0, 4, 1	11	0.003	0.0040
SMM-LILLE[h]	150–660	0, 63, 30	2890	0.030–0.050	0.0277
SMM-LILLE[h]	150–660	0, 52, 29	179	0.100	0.0788
OSLO	7–80	0, 33, 8	137	0.150	
OSLO	7–80		3	0.200	0.1343
SMM-LILLE[h]	150–660	0, 38, 29	38	0.200	

Notes. [(a)] Parameter values are given in Table 5. The observed minus calculated residuals are given in the supplementary Table S2. [(b)] Sources of data: FTMW-LILLE, SMM-LILLE and OSLO data comes from present work, see experimental section. [(c)] Range containing the measurements in a given row. [(d)] v_t state and maximum J and K_a for each group of measurements. [(e)] Number of MW lines in each uncertainty group. [(f)] One-sigma standard uncertainty in MHz used in the fit. [(g)] Root-mean-square deviation in MHz for each group. [(h)] The SMM-LILLE spectrometer spectral ranges for these measurements are 150–322 GHz, 400–533 GHz and 583–660 GHz.

Table 3. Comparison of results of the fits using the code BELGI for the various isotopologues of methyl formate, using the same RAM method.

Molecules	V_3	F	s[a]	ρ[b]	θ_{RAM}[c]	$\langle(i,a)$[d]	J_{max}	K_a^{max}	v_t^{max}	N[e]	N_p[f]	rms[g]	Ref.
$HC^{18}OOCH_3$	392	5.5[fixed]	32	0.0798	26	55	63	30	0	3258	29	0.82	Present work
$HCO^{18}OCH_3$	391	5.5[fixed]	32	0.0806	26	54	62	30	0	4430	30	0.60	Present work
$HCOO^{13}CH_3$	407	5.7[fixed]	32	0.0845	24	52	63	34	0	936	27	1.08	Carvajal et al. (2009)
$DCOOCH_3$	389	5.5[fixed]	31	0.0813	24	51	64	36	0	1703	24	1.11	Margulès et al. (2010)
$H^{12}COO^{12}CH_3$	373	5.5	30	0.0842	25	53	62	26	1	10533	55	0.71	Ilyushin et al. (2009)
$H^{13}COOCH_3$	372	5.5	30	0.0841	25	52	59	27	1	7445	45	0.55	Carvajal et al. (2010)

Notes. [(a)] Reduced height $s = 4V_3/9F$ (unitless). [(b)] Coupling constant between internal and global rotation (unitless). [(c)] Angle between the rho-axis system and the principal axis system, for C_s molecules, in degrees. [(d)] Angle between the methyl top symmetry axis and the a principal axis, in degrees. [(e)] Number of lines included in the fit. [(f)] Number of parameters used in the fit. [(g)] Unitless Root-mean-square deviations, which should be 1.0 if the fit were good to experimental uncertainty.

is fixed to its ab initio value calculated in the equilibrium structure at the CCSD(T)/cc-pV5Z + core-correction level of theory (5.69 cm^{-1}), whereas for $DCOOCH_3$ and the two ^{18}O-methyl formate species, F is fixed to the ground state $v_t = 0$ value of the normal species (5.49 cm^{-1}). Finally, for the $^{13}C_2$-methyl formate, $DCOOCH_3$ and the ^{18}O isotopologues, the V_6 parameter, which is the second term in the torsional potential Fourier series

$$V(\gamma) = \frac{V_3}{2} \times (1 - \cos 3\gamma) + \frac{V_6}{2} \times (1 - \cos 6\gamma) + \cdots$$

Table 4. Torsion-rotation parameters needed for the global fit of transitions involving $v_t = 0$ torsional energy levels of $HCO^{18}OCH_3$ methyl formate.

nlm[a]	Operator[b]	Parameter	$HCO^{18}OCH_3$[c]	nlm	Operator	Parameter	$HCO^{18}OCH_3$[c]
220	$(1-\cos 3\gamma)/2$	V_3	391.35594(377)	404	$-P^4$	D_J	$-0.1781(240)\times10^{-7}$
	P_γ^2	F	5.49038[d]		$-P^2P_a^2$	D_{JK}	$-0.13188(145)\times10^{-5}$
211	$P_\gamma P_a$	ρ	0.08057980(284)		$-P_a^4$	D_K	$0.50871(198)\ 10^{-5}$
202	P_a^2	A^{RAM}	0.56177506(636)		$-2P^2(P_b^2-P_c^2)$	δ_J	$-0.4338(120)\times10^{-7}$
	P_b^2	B^{RAM}	0.30985885(512)		$-\{P_a^2,(P_b^2-P_c^2)\}$	δ_K	$0.2660(229)\times10^{-7}$
	P_c^2	C^{RAM}	0.174524916(392)		$P^2(P_aP_b+P_bP_a)$	D_{abJ}	$-0.93534(382)\times10^{-6}$
	$(P_a\ P_b+P_b\ P_a)$	D_{ab}	−0.16362225(395)		$(P_a^3\ P_b+P_b\ P_a^3)$	D_{abK}	$0.153543(349)\times10^{-5}$
422	$\sin 3\gamma\ (P_b\ P_c+P_c\ P_b)$	D_{bc}	0.00197000(784)	624	$(1-\cos 3\gamma)P_a^4$	k_{5K}	$-0.2211(122)\times10^{-6}$
	$(1-\cos 3\gamma)\ P^2$	F_v	−0.00248015(206)	606	P^6	H_J	$0.3554(355)\times10^{-12}$
	$(1-\cos 3\gamma)\ P_a^2$	k_5	0.0127104(136)		$P^4\ P_a^2$	H_{JK}	$0.6789(118)\ \ 10^{-11}$
	$(1-\cos 3\gamma)(P_a\ P_b+P_b\ P_a)$	d_{ab}	−0.00627264(369)		P_a^6	H_K	$0.52885(929)\times10^{-10}$
413	$P_\gamma\ P_a^3$	k_1	$0.48356(550)\ \ 10^{-5}$		$2P^4(P_b^2-P_c^2)$	h_J	$0.1855(169)\times10^{-12}$
	$P_\gamma\ P_a\ P^2$	L_v	$0.17553(349)\ \ 10^{-5}$		$\{P_a^4,(P_b^2-P_c^2)\}$	h_K	$0.17745(887)\times10^{-11}$
	$P_\gamma\ \{P_a\ ,(P_b^2-P_c^2)\}$	c_4	$0.13412(118)\ \ 10^{-5}$		$P^2\ (P_a^3\ P_b+P_b\ P_a^3)$	D_{abJK}	$0.3103(210)\times10^{-11}$
	$P_\gamma\ (P_a^2\ P_b+P_b\ P_a^2)$	δ_{ab}	$-0.18642(438)\ 10^{-5}$		$P^4\ (P_a\ P_b+P_b\ P_a)$	D_{abJJ}	$-0.17323(825)\times10^{-11}$
				615	$P^2\ P_\gamma\ P_a^3$	k_{1J}	$-0.39079(975)\times10^{-9}$

Notes. [a] Notation from Ilyushin et al. (2008); $n = l + m$, where n is the total order of the operator, l is the order of the torsional part and m is the order of the rotational part. [b] Notation from Ilyushin et al. (2008). $\{A, B\} = AB + BA$. The product of the parameter and operator from a given row yields the term actually used in the vibration-rotation-torsion Hamiltonian, except for F, ρ and A^{RAM}, which occur in the Hamiltonian in the form $F\ (P_\gamma - \rho P_a)^2 + A^{RAM}P_a^2$. [c] Present work. [d] Value of the internal rotation constant F was kept fixed to the $HCOOCH_3$ value from Carvajal et al. (2007).

cannot be determined. This V_6 term is fairly high for normal methyl formate ($23.9018(636)\ cm^{-1}$) and we expect its value to be of the same magnitude for the other methyl formate species. However, in the absence of excited torsional transitions we cannot fit V_6 parameter in the cases of $^{13}C_2$-methyl formate, $DCOOCH_3$ or for the ^{18}O isotopologues; we fixed its value to zero. For these reasons, the values of V_3 determined for these methyl formate isotopologues can only be considered as effective values that contain the contribution of V_6.

The two ^{18}O-methyl formate species show excellent root-mean-square deviations (rms). For $HC^{18}OOCH_3$, however, many lines were overlapped by transitions originated from the methanol molecule used during the synthesis and was still present in very small amounts in the sample even though it was purified (see experimental section). Therefore less lines were available for the analysis of the $HC^{18}OOCH_3$ isotopologue than for the $HCO^{18}OCH_3$ isotopologue. Tables 4 and 5 show the 31 and 30 parameters (including the fixed parameter F) used in our fit of the ground torsional state of the $HCO^{18}OCH_3$ and $HC^{18}OOCH_3$ species. The two sets of parameters are similar.

5. Line strengths

The intensity calculations for the two ^{18}O species of methyl formate were performed using the same method as described in Hougen et al. (1994); Ilyushin et al. (2008), and applied for the normal species by Carvajal et al. (2007), the ^{13}C species (Carvajal et al. 2009, 2010) and for $DCOOCH_3$ (Margulès et al. 2010). For this reason we will not repeat it here. The line strength calculation for the ^{18}O species was performed using the same value for the dipole moment as for the parent methyl formate (Margulès et al. 2010). This assumption was made because the angle between the internal axis of the methyl top and the principal a-axis does not change much upon substitution (see the $<(i,a)$ angle values in Table 6). All other structural parameters such as the angle between RAM and PAM axes (θ_{RAM}) and the ρ parameter do not change much upon substitution (see Table 6). Because the changes in the structure in the various isotopomers are not important, we assumed that the dipole moment does not change considerably from one species to another. The dipole moment components of $HCO^{18}OCH_3$ and $HC^{18}OOCH_3$ in RAM axis system that we used for the intensity calculations are $\mu_a^{RAM} = 1.790$ D; $\mu_b^{RAM} = -0.094$ D and $\mu_a^{RAM} = 1.791$ D; $\mu_b^{RAM} = -0.081$ D, respectively.

We provided Tables A1 and A2, which are part of the supplementary Tables S1 and S2 (available on CDS) in the appendix. They contain all included lines from our fit for the $HCO^{18}OCH_3$ and $HC^{18}OOCH_3$ methyl formate species. They show the line assignments, the observed frequencies with measurement uncertainty (in parenthesis), the computed frequencies, observed-calculated values, the line strength for the $v_t = 0$ transitions, and the lower-state energy relative to the $J = K = 0$ A-species level taken as zero-energy level.

6. ^{18}O-$HCOOCH_3$ detection in Orion KL

Thanks to the new laboratory frequencies provided above, we have detected the two ^{18}O isotopologues of $HCOOCH_3$ in the IRAM 30 m line survey of Orion KL presented in Tercero et al. (2010, 2011). After summarizing the observations, data reduction, and overall results of that line survey (Sect. 6.1), we concentrated on the detection of the two ^{18}O isotopologues of $HCOOCH_3$ and their analysis (Sect. 6.2). This is the last of a series of papers dedicated to the different isotopologues of methyl formate (laboratory frequencies and detection in Orion KL, see Carvajal et al. 2009; and Margulès et al. 2010).

Table 5. Torsion-rotation parameters needed for the global fit of transitions involving $v_t = 0$ torsional energy levels of $HC^{18}OOCH_3$ methyl formate.

nlm[a]	Operator[b]	Parameter	$HC^{18}OOCH_3$[c]	nlm	Operator	Parameter	$HC^{18}OOCH_3$[c]
220	$(1-\cos 3\gamma)/2$	V_3	391.56929 (646)	404	$-P^4$	D_J	$0.2097(211)\times10^{-7}$
	P_γ^2	F	5.49038[d]		$-P^2\ P_a^2$	D_{JK}	$-0.180042(857)\times10^{-5}$
211	$P_\gamma P_a$	ρ	0.07977981(403)		$-P_a^4$	D_K	$0.532763(931)\times10^{-5}$
202	P_a^2	A^{RAM}	0.56776348 (810)		$-2P^2(P_b^2-P_c^2)$	δ_J	$-0.2519(106)\times10^{-7}$
	P_b^2	B^{RAM}	0.30216119(677)		$-\{P_a^2,(P_b^2-P_c^2)\}$	δ_K	$-0.35754(981)\times10^{-7}$
	P_c^2	C^{RAM}	0.170313544(770)		$P^2\ (P_aP_b+P_bP_a)$	D_{abJ}	$-0.90979(301)\times10^{-6}$
	$(P_aP_b+P_bP_a)$	D_{ab}	−0.16731097(526)		$(P_a^3P_b+P_bP_a^3)$	D_{abK}	$0.144807(244)\times10^{-5}$
422	$\sin 3\gamma(P_bP_c+P_cP_b)$	D_{bc}	0.0017299(105)	624	$(1-\cos 3\gamma)P^2\ P_a^2$	k_{5J}	$-0.14491(670)\times10^{-6}$
	$P_\gamma^2\ P_a^2$	k_2	$0.35429(548)\ 10^{-4}$		$P^2\ P_\gamma^2\ P_a^2$	k_{2J}	$-0.28717(908)\times10^{-8}$
	$(1-\cos 3\gamma)\ P^2$	F_v	−0.00203120(379)	606	$P^4\ P_a^2$	H_{JK}	$0.6870(113)\times10^{-11}$
	$(1-\cos 3\gamma)\ P_a^2$	k_5	0.0140399(189)		$P^2\ P_a^4$	H_{KJ}	$-0.23719(718)\times10^{-10}$
	$(1-\cos 3\gamma)(P_aP_b+P_bP_a)$	d_{ab}	−0.00613830(453)		P_a^6	H_K	$0.68402(464)\times10^{-10}$
	$P_\gamma^2\ P^2$	G_V	$0.118883(538)\ 10^{-4}$		$2P^4(P_b^2-P_c^2)$	h_J	$0.935(9)\times10^{-14}$
413	$P_\gamma\{P_a,(P_b^2-P_c^2)\}$	c_4	$0.11880(160)\ 10^{-5}$		$P^2\ (P_a^3P_b+P_bP_a^3)$	D_{abJK}	$0.5012(136)\times10^{-11}$
	$P_\gamma(P_a^2P_b+P_bP_a^2)$	δ_{ab}	$-0.21412\ (315)\ \ 10^{-5}$		$P^4\ (P_aP_b+P_bP_a)$	D_{abJJ}	$-0.8718(390)\times10^{-12}$

Notes. [a] Notation from Ilyushin et al. (2008); $n = l + m$, where n is the total order of the operator, l is the order of the torsional part and m is the order of the rotational part. [b] Notation from Ilyushin et al. (2008). $\{A, B\} = AB + BA$. The product of the parameter and operator from a given row yields the term actually used in the vibration-rotation-torsion Hamiltonian, except for F, ρ and A^{RAM}, which occur in the Hamiltonian in the form $F\,(P_\gamma - \rho P_a)^2 + A^{RAM}P_a^2$. [c] Present work. [c] Value of the internal rotation constant F was kept fixed to the $HCOOCH_3$ value from Carvajal et al. (2007).

Table 6. Rotational constants in the RHO axis system (RAM) and in the principal axis system (PAM) for $HC^{18}OOCH_3$ and $HCO^{18}OCH_3$.

	$HC^{18}OOCH_3$		$HCO^{18}OCH_3$	
	(RAM)[a]	(PAM)[b]	(RAM)[a]	(PAM)[b]
A(MHz)	17021.121(243)	19443.700(236)	16841.593(191)	19255.846(182)
B(MHz)	9058.565(203)	6635.985(211)	9289.335(153)	6875.081(160)
C(MHz)	5105.8716 (231)	5105.8716 (231)	5232.1254(118)	5232.1254(118)
D_{ab}(MHz)	−5015.857 (158)		−4905.272(118)	
$<(i,a)$		54.754(2)		54.042 (1)
$<(i,b)$		35.246(2)		35.958 (1)
$<(i,c)$		90.000		90.000
θ_{RAM}[c]		25.7798(7)		26.2053(6)

Notes. Angles between the principal axis and the methyl top axis. [a] Rotational constants obtained in our work for RAM-axis system (see Tables 4 and 5 for $HCO^{18}OCH_3$ and $HC^{18}OOCH_3$). [b] Rotational constants of our work transformed to the principal axis system and angles in degrees between the principal axis (a, b, c) and the methyl top axis (i). [c] The angle θ_{RAM} angle between the a-principal axis and the a-RAM axis is given in degrees and obtained from Eq. (1) of Carvajal et al. (2007) with the parameters A^{RAM}, B^{RAM}, C^{RAM}, and D_{ab} of Tables 4 and 5.

6.1. Observations, data reduction, and overall results of the line survey

The observations were carried out using the IRAM 30m radio telescope during September 2004 (3 mm and 1.3 mm windows), March 2005 (full 2 mm window), April 2005 (completion of 3 mm and 1.3 mm windows), and January 2007 (maps and pointed observations at particular positions). Four SiS receivers operating at 3, 2, and 1.3 mm were used simultaneously with image sideband rejections within 20–27 dB (3 mm receivers), 12–16 dB (2 mm receivers) and ≃13 dB (1.3 mm receivers). System temperatures were in the range 100–350 K for the 3 mm receivers, 200–500 K for the 2 mm receivers, and 200–800 K for the 1.3 mm receivers, depending on the particular frequency, weather conditions, and source elevation. For frequencies in the range 172–178 GHz, the system temperature was significantly higher, 1000–4000 K, owing to proximity of the atmospheric water line at 183.31 GHz. The intensity scale was calibrated using two absorbers at different temperatures and the atmospheric transmission model (ATM, Cernicharo 1985; Pardo et al. 2001).

Pointing and focus were regularly checked on the nearby quasars 0420–014 and 0528+134. Observations were made in the balanced wobbler-switching mode, with a wobbling frequency of 0.5 Hz and a beam throw in azimuth of ±240″. No contamination from the off-position affected our observations except for a marginal one at the lowest elevations (∼25°) for molecules showing low J emission along the extended ridge.

Two filter banks with 512 × 1 MHz channels and a correlator providing two 512 MHz bandwidths and 1.25 MHz resolution

were used as backends. We pointed towards the IRc2 source at $\alpha_{2000.0} = 5^h35^m14.5^s$, $\delta_{2000.0} = -5°22'30.0''$ (J2000.0).

Although we had a good receiver image-band rejection, each setting was repeated at a slightly shifted frequency (10–20 MHz) to manually identify and remove all features arising from the image side band. The spectra from different frequency settings were used to identify all potential contaminating lines from the image side band. In some cases it was impossible to eliminate the contribution of the image side band and we removed the signal in those contaminated channels, leaving holes in the data. The total frequencies blanked this way represent less than 0.5% of the total frequency coverage. We removed most of the features from the image side band above a 0.05 K threshold.

Within the 168 GHz bandwidth covered (80–115.5, 130–178, and 196–281 GHz), we detected more than 14 600 spectral features of which ~10 200 were already identified and attributed to 43 molecules, including 148 different isotopologues and vibrationally excited states. Any feature covering more than 3–4 channels and of intensity greater than 0.02 K is above 3σ and was considered to be a line in our survey. In the 2 mm and 1.3 mm windows the features weaker than 0.1 K have not yet been systematically analysed, except when searching for isotopic species with good laboratory frequencies. We therefore expect to considerably increase the number of both identified and unidentified lines. We note that the number of U lines was initially much larger. Identification of some isotopologues of most abundant species allowed us to reduce the number of U-lines at a rate of ~500 lines per year (see, as examples, Demyk et al. 2007; Margulès et al. 2009b; Carvajal et al. 2009; and Margulès et al. 2010). We used standard procedures to identify lines above 0.2 K including all possible contributions (taking into account the energy of the transition and the line strength) from different species. Thanks to the wide frequency coverage of our survey, many rotational lines were observed for each species, hence it is possible to estimate the contribution of a given molecule to the intensity of a spectral feature where several lines from different species are blended.

In agreement with previous works, four different spectral cloud components were defined in the analysis of low angular resolution line surveys of Orion KL where different physical components overlap in the beam. These components are characterized by different physical and chemical conditions (Blake et al. 1987; Blake et al. 1996; Tercero et al. 2010, 2011): (i) a narrow or "spike" (~4 km s^{-1} line-width) component at $v_{LSR} \simeq 9$ km s^{-1} delineating a north-to-south *extended ridge* or ambient cloud ($T_k \simeq 60$ K, $n(H_2) \simeq 10^5$ cm^{-3}); (ii) a compact and quiescent region, the *compact ridge*, ($v_{LSR} \simeq 8$ km s^{-1}, $\Delta v \simeq 3$ km s^{-1}, $T_k \simeq 110$ K, $n(H_2) \simeq 10^6$ cm^{-3}) identified for the first time by Johansson et al. (1984); (iii) the *plateau*, a mixture of outflows, shocks, and interactions with the ambient cloud ($v_{LSR} \simeq 6-10$ km s^{-1}, $\Delta v \gtrsim 25$ km s^{-1}, $T_k \simeq 150$ K, $n(H_2) \simeq 10^6$ cm^{-3}); (iv) a *hot core* component ($v_{LSR} \simeq 5$ km s^{-1}, $\Delta v \sim 10$ km s^{-1}, $T_k \simeq 225$ K, $n(H_2) \simeq 5 \times 10^7$ cm^{-3}) first detected in ammonia emission Morris et al. (1980). Methyl formate (in general, organic saturated O-rich molecules) emission comes mainly from the compact ridge component.

6.2. Detection and astronomical modelling

We have detected the ^{18}O isotopologues of $HCOOCH_3$ in states A and E through 80 emission lines of the line survey. Despite the large number of line blends in the 80–280 GHz domain, we were able to assign these 80 lines to $HCO^{18}OCH_3$ and $HC^{18}OOCH_3$. Table 7 gives the observed line intensities and frequencies together with the predicted frequencies from the rotational constants derived in this paper for all lines of these isotopologues that are not strongly blended with other lines from other species. All emission lines expected to have a T_{MB} above 0.1 K (those lines that correspond with the overlap of different *a*-type transitions with $K_a = 0, 1$ in the 1.3 mm domain) were detected. Unfortunately, several of them are blended with strong emission lines from other molecules; Table 7 gives information on these contaminating lines. There is no strong line expected that is not observed in the astronomical spectra. In addition, Table 7 gives the line intensity derived from the model predictions (see below). The observed brightness temperature for the lines in Table 7 has been obtained from the peak emission channel in the spectra. To quantify the contribution of possible blending, all contaminating species should be modelled. Hence, we limited ourselves in Table 7 to those lines that are practically free of blending or that only are affected by other weak lines. Consequently, our observed main beam temperatures have to be considered as upper limits for these weakly blended lines. The predicted intensities agree quite well with the observations of the 80 spectral lines detected, with 40 lines practically free of blending with other species.

All together these observations ensure the detection of ^{18}O-methyl formate in Orion KL.

Figures 1 and 2 show selected detected lines at 3 and 2 mm and at 1.3 mm, respectively, together with our best model (see below). In those figures we have tried to display no strongly contaminated lines (at least one per box). The overlaps with other species are quoted in Table 7. In addition, both figures show many detected lines without blending with other species, which support the first detection in space of both ^{18}O methyl formate isotopologues.

Following the models made by Margulès et al. (2010), we consider that the line profiles of methyl formate display the four components of Orion KL quoted above. We added an additional component for the compact ridge with a kinetic temperature of 250 K to better reproduce the line profiles of all isotopologues of $HCOOCH_3$ in all spectral windows of the 30-m survey (this inner and hotter component of the compact ridge is required for fitting the emission lines of different molecules in the HIFI domain on-board the *Herschel* Space Observatory; Tercero et al. and Marcelino et al. both in prep.). Because of the weakness of ^{18}O methyl formate lines, the plateau component is not needed to reproduce the observations of these isotopologues. Therefore, in this case, we assume that the emission of ^{18}O methyl formate comes from the compact ridge, "hot" compact ridge, extended ridge, and hot core.

We used LTE approximation in all cases (for the extended ridge, both compact ridges, and hot core). The lack of collisional rates for this molecule prevents a more detailed analysis of the emission of methyl formate. Nevertheless, taking into account the physical conditions of the different cloud components, we expect that this approximation works reasonably well. Only for the extended ridge we were able to obtain non LTE conditions. However, the lines affected by this cloud component are those involving low-energy levels, for which its contribution is less than 50%. Its effect on the lines associated with high-energy levels is negligible.

For each cloud component we assumed uniform physical conditions for the kinetic temperature, density, radial velocity, and line width (see parameters quoted in Sect. 6.1). We adopted these values from the data analysis (Gaussian fits and an attempt to simulate the line profiles for several molecules with LTE

Table 7. Detected lines of ^{18}O-HCOOCH$_3$.

Species	Transition J_{K_a,K_c}	Rest freq. (MHz)	E_u (K)	S_{ij}	Observed freq. (MHz)	Observed T_{MB} (K)	Modeled T_{MB} (K)
A-HCO^{18}OCH$_3$	$7_{2,6}$-$6_{2,5}$	83327.49	18.7	6.40	83327.5	0.012	0.013
E-HC^{18}OOCH$_3$	$8_{1,8}$-$7_{1,7}$	85805.17	19.4	7.86	85802.4[1]	0.030	0.016
A-HC^{18}OOCH$_3$	$8_{1,8}$-$7_{1,7}$	85807.01	19.4	7.86	85807.4	0.033	0.016
E-HCO^{18}OCH$_3$	$8_{2,7}$-$7_{2,6}$	94754.73	23.2	7.49	94755.5	0.037	0.017
E-HC^{18}OOCH$_3$	$8_{3,5}$-$7_{3,4}$	95996.47	26.4	6.90	95996.5	0.025	0.016
E-HC^{18}OOCH$_3$	$8_{1,7}$-$7_{1,6}$	96466.39	21.8	7.79	96466.5	0.025	0.017
A-HCO^{18}OCH$_3$	$8_{3,6}$-$7_{3,5}$	97429.39	26.7	6.87	97430.0[1]	0.031	0.016
E-HCO^{18}OCH$_3$	$8_{4,5}$-$7_{4,4}$	97569.09	31.2	5.76	97569.5	0.028	0.013
E-HCO^{18}OCH$_3$	$9_{0,9}$-$8_{0,8}$	99039.16	24.5	8.86	99040.0	0.025	0.022
A-HCO^{18}OCH$_3$	$9_{0,9}$-$8_{0,8}$	99040.86	24.5	8.86	[2]	...	...
A-HCO^{18}OCH$_3$	$8_{2,6}$-$7_{2,5}$	102414.82	24.3	7.53	102415.0	0.029	0.019
E-HCO^{18}OCH$_3$	$9_{2,8}$-$8_{2,7}$	106025.11	28.3	8.52	106025.5	0.025	0.023
E-HC^{18}OOCH$_3$	$9_{5,4}$-$8_{5,3}$	106251.00	41.8	6.24	106251.0	0.037	0.014
A-HC^{18}OOCH$_3$	$9_{5,4}$-$8_{5,3}$	106265.60	41.8	6.24	106265.4	0.050	0.013
E-HC^{18}OOCH$_3$	$9_{3,7}$-$8_{3,6}$	106295.64	31.6	8.01	106295.5	0.044	0.020
A-HC^{18}OOCH$_3$	$9_{3,7}$-$8_{3,6}$	106302.47	31.4	8.01	106302.5	0.025	0.021
E-HC^{18}OOCH$_3$	$9_{4,6}$-$8_{4,5}$	106576.35	36.0	6.86	106576.5	0.019	0.017
E-HC^{18}OOCH$_3$	$9_{1,8}$-$8_{1,7}$	107284.86	27.0	8.75	107284.4	0.038	0.025
A-HC^{18}OOCH$_3$	$9_{1,8}$-$8_{1,7}$	107292.37	27.0	8.75	107292.5	0.038	0.023
E-HC^{18}OOCH$_3$	$9_{3,6}$-$8_{3,5}$	108822.96	31.9	8.01	108823.5	0.038	0.023
E-HCO^{18}OCH$_3$	$10_{1,10}$-$9_{1,9}$	109037.62	29.8	9.85	109037.5	0.038	0.027
A-HCO^{18}OCH$_3$	$10_{1,10}$-$9_{1,9}$	109039.39	29.8	9.85	109040.6[1]	0.057	0.027
E-HCO^{18}OCH$_3$	$10_{0,10}$-$9_{0,9}$	109365.53	29.8	9.85	109365.5[1]	0.032	0.028
E-HCO^{18}OCH$_3$	$9_{1,8}$-$8_{1,7}$	109988.47	27.7	8.71	109988.5	0.038	0.026
A-HC^{18}OOCH$_3$	$9_{2,7}$-$8_{2,6}$	111644.35	29.0	8.58	111644.5	0.025	0.024
E-HC^{18}OOCH$_3$	$10_{2,9}$-$9_{2,8}$	114108.78	33.1	9.56	114108.5	0.025	0.026
E-HCO^{18}OCH$_3$	$12_{0,12}$-$11_{0,11}$	130114.40	42.7	11.9	130115.1[1]	0.012	0.038
A-HCO^{18}OCH$_3$	$12_{0,12}$-$11_{0,11}$	130115.91	41.7	11.9	[2]	...	...
E-HC^{18}OOCH$_3$	$12_{2,11}$-$11_{2,10}$	135472.80	45.6	11.6	135472.7	0.026	0.036
E-HC^{18}OOCH$_3$	$13_{0,13}$-$12_{0,12}$	137256.72	48.6	12.9	137256.3	0.080	0.044
A-HC^{18}OOCH$_3$	$13_{0,13}$-$12_{0,12}$	137258.10	47.4	12.9	[2]	...	0.044
E-HCO^{18}OCH$_3$	$11_{3,8}$-$10_{3,7}$	139979.02	45.1	10.2	139978.6	0.046	0.031
A-HCO^{18}OCH$_3$	$11_{3,8}$-$10_{3,7}$	139995.37	45.1	10.2	139995.7	0.026	0.031
E-HCO^{18}OCH$_3$	$13_{1,13}$-$12_{1,12}$	140452.90	49.9	12.9	140453.3	0.073	0.045
A-HCO^{18}OCH$_3$	$13_{1,13}$-$12_{1,12}$	140454.43	48.5	12.9	[2]	...	0.043
E-HC^{18}OOCH$_3$	$13_{2,12}$-$12_{2,11}$	145979.69	52.6	12.6	145980.5[1]	0.12	0.038
A-HC^{18}OOCH$_3$	$13_{2,12}$-$12_{2,11}$	145985.77	52.6	12.6	145985.6[3]	0.055	0.037
E-HCO^{18}OCH$_3$	$12_{7,6}$-$11_{7,5}$	146004.17	76.6	7.93	146004.1	0.040	0.049
A-HCO^{18}OCH$_3$	$12_{7,6}$-$11_{7,5}$	146004.24	76.6	7.93	[2]	...	...
A-HCO^{18}OCH$_3$	$12_{7,5}$-$11_{7,4}$	146004.47	77.2	7.93	[2]	...	...
E-HC^{18}OOCH$_3$	$12_{2,10}$-$11_{2,9}$	147364.51	48.6	11.6	147363.8	0.085	0.038
E-HC^{18}OOCH$_3$	$14_{1,14}$-$13_{1,13}$	147369.38	56.2	13.9	147371.3[4]	0.11	0.048
A-HC^{18}OOCH$_3$	$14_{1,14}$-$13_{1,13}$	147370.78	54.4	13.9	[2]	...	0.049
A-HC^{18}OOCH$_3$	$12_{2,10}$-$11_{2,9}$	147377.44	54.4	11.6	147377.0	0.11	0.038
E-HC^{18}OOCH$_3$	$14_{0,14}$-$13_{0,13}$	147423.20	56.2	13.9	147423.8[1]	0.22	0.050
A-HC^{18}OOCH$_3$	$14_{0,14}$-$13_{0,13}$	147424.53	54.4	13.9	[2]	...	...
E-HCO^{18}OCH$_3$	$14_{0,14}$-$13_{0,13}$	150934.10	57.7	13.9	150934.6	0.11	0.052
A-HCO^{18}OCH$_3$	$14_{0,14}$-$13_{0,13}$	150935.51	55.7	13.9	[2]	...	...
E-HC^{18}OOCH$_3$	$13_{4,10}$-$12_{4,9}$	154549.58	62.4	11.8	154550.1	0.062	0.038
E-HCO^{18}OCH$_3$	$13_{3,11}$-$12_{3,10}$	156545.98	58.7	12.6	156546.5	0.056	0.039
E-HCO^{18}OCH$_3$	$13_{7,7}$-$12_{7,6}$	158334.49	84.2	9.26	158335.0	0.034	0.053
A-HCO^{18}OCH$_3$	$13_{7,7}$-$12_{7,6}$	158334.52	84.2	9.26	[2]	...	...
E-HCO^{18}OCH$_3$	$13_{7,6}$-$12_{7,5}$	158335.25	84.2	9.26	[2]	...	...
A-HC^{18}OOCH$_3$	$14_{10,5}$-$13_{10,4}$	164877.29	124.8	6.86	164877.6	0.058	0.018
A-HC^{18}OOCH$_3$	$14_{10,4}$-$13_{10,3}$	164877.29	124.8	6.86	[2]	...	...
A-HCO^{18}OCH$_3$	$13_{3,10}$-$12_{3,9}$	166818.88	60.5	12.4	166819.5[1]	0.070	0.042
E-HC^{18}OOCH$_3$	$16_{0,16}$-$15_{0,15}$	167776.18	72.9	15.9	167778.5[1]	0.10	0.066
A-HC^{18}OOCH$_3$	$16_{0,16}$-$15_{0,15}$	167777.40	70.0	15.9	[2]	...	...
E-HCO^{18}OCH$_3$	$14_{6,8}$-$13_{6,7}$	171239.76	84.3	11.4	171240.1	0.021	0.029
E-HCO^{18}OCH$_3$	$16_{1,16}$-$15_{1,15}$	171768.46	74.8	15.9	171769.5	0.10	0.067
A-HCO^{18}OCH$_3$	$16_{1,16}$-$15_{1,15}$	171769.77	71.7	15.9	[2]	...	...
E-HCO^{18}OCH$_3$	$14_{5,9}$-$13_{5,8}$	172580.99	77.5	12.2	172580.5	0.13	0.034
A-HCO^{18}OCH$_3$	$14_{5,9}$-$13_{5,8}$	172605.81	77.5	12.2	172606.5	0.14	0.034

Table 7. continued.

Species	Transition J_{K_a,K_c}	Rest freq. (MHz)	E_u (K)	S_{ij}	Observed freq. (MHz)	Observed T_{MB} (K)	Modeled T_{MB} (K)
E-HC^{18}OOCH$_3$	$19_{1,19}$-$18_{1,18}$	198318.71	101.5	18.9	198321.1	0.10	0.080
A-HC^{18}OOCH$_3$	$19_{1,19}$-$18_{1,18}$	198319.77	97.1	18.9	[2]	...	...
E-HC^{18}OOCH$_3$	$19_{0,19}$-$18_{0,18}$	198321.96	101.5	18.9	[2]	0.082	
A-HC^{18}OOCH$_3$	$19_{0,19}$-$18_{0,18}$	198323.01	97.1	18.9	[2]	...	...
E-HC^{18}OOCH$_3$	$17_{2,15}$-$16_{2,14}$	198878.18	91.5	16.4	198877.3[1]	0.069	0.046
A-HC^{18}OOCH$_3$	$17_{2,15}$-$16_{2,14}$	198886.46	91.5	16.4	198888.5[5]	0.060	0.046
A-HC^{18}OOCH$_3$	$17_{6,11}$-$16_{6,10}$	202607.55	110.5	14.9	202608.1[6]	0.076	0.031
E-HCO^{18}OCH$_3$	$19_{1,19}$-$18_{1,18}$	203058.14	104.1	18.9	203059.4	0.16	0.11
A-HCO^{18}OCH$_3$	$19_{1,19}$-$18_{1,18}$	203059.27	99.5	18.9	[2]	...	...
E-HCO^{18}OCH$_3$	$19_{0,19}$-$18_{0,18}$	203060.03	104.1	18.9	[2]	...	...
A-HCO^{18}OCH$_3$	$19_{0,19}$-$18_{0,18}$	203061.15	99.5	18.9	[2]	...	....
E-HC^{18}OOCH$_3$	$20_{1,20}$-$19_{1,19}$	208502.31	112.0	19.9	[7]	...	0.11
A-HC^{18}OOCH$_3$	$20_{1,20}$-$19_{1,19}$	208503.31	107.1	19.9	[2]	...	...
E-HC^{18}OOCH$_3$	$20_{0,20}$-$19_{0,19}$	208504.12	112.0	19.9	[2]	...	...
A-HC^{18}OOCH$_3$	$20_{0,20}$-$19_{0,19}$	208505.12	107.1	19.9	[2]	...	...
A-HC^{18}OOCH$_3$	$18_{11,8}$-$17_{11,7}$	212218.60	175.8	11.3	212219.8	0.071	0.025
A-HC^{18}OOCH$_3$	$18_{11,7}$-$17_{11,6}$	212218.60	175.8	11.3	[2]	...	...
E-HCO^{18}OCH$_3$	$20_{1,20}$-$19_{1,19}$	213485.36	114.8	19.9	[1]	...	0.16
E-HCO^{18}OCH$_3$	$20_{0,20}$-$19_{0,19}$	213486.38	114.8	19.9	[2]	...	...
A-HCO^{18}OCH$_3$	$20_{1,20}$-$19_{1,19}$	213486.42	109.7	19.9	[2]	...	...
A-HCO^{18}OCH$_3$	$20_{0,20}$-$19_{0,19}$	213487.44	109.7	19.9	[2]	...	...
E-HC^{18}OOCH$_3$	$18_{7,11}$-$17_{7,10}$	213740.59	129.0	15.2	213741.1	0.045	0.052
A-HC^{18}OOCH$_3$	$18_{7,12}$-$17_{7,11}$	213741.50	129.0	15.3	[2]	...	...
E-HC^{18}OOCH$_3$	$18_{6,13}$-$17_{6,12}$	214582.20	120.8	15.9	214583.6[1]	0.15	0.065
A-HC^{18}OOCH$_3$	$18_{6,13}$-$17_{6,12}$	214582.20	120.7	16.0	[2]	...	...
E-HC^{18}OOCH$_3$	$21_{1,21}$-$20_{1,20}$	218684.67	122.9	20.9	[8]	...	0.16
A-HC^{18}OOCH$_3$	$21_{1,21}$-$20_{1,20}$	218685.61	117.6	20.9	[2]	...	...
E-HC^{18}OOCH$_3$	$21_{0,21}$-$20_{0,20}$	218685.68	122.9	20.9	[2]	...	...
A-HC^{18}OOCH$_3$	$21_{0,21}$-$20_{0,20}$	218686.61	117.6	20.9	[2]	...	...
E-HCO^{18}OCH$_3$	$21_{1,21}$-$20_{1,20}$	223911.47	126.0	20.9	[9]	...	0.18
E-HCO^{18}OCH$_3$	$21_{0,21}$-$20_{0,20}$	223912.01	126.0	20.9	[2]	...	...
A-HCO^{18}OCH$_3$	$21_{1,21}$-$20_{1,20}$	223912.48	120.5	20.9	[2]	...	...
A-HCO^{18}OCH$_3$	$21_{0,21}$-$20_{0,20}$	223913.02	120.5	20.9	[2]	...	...
A-HC^{18}OOCH$_3$	$19_{8,12}$-$18_{8,11}$	225191.38	149.5	15.7	225194.9	0.15	0.028
E-HC^{18}OOCH$_3$	$19_{8,12}$-$18_{8,11}$	225194.04	149.5	15.7	[2]	...	0.048
A-HC^{18}OOCH$_3$	$19_{8,11}$-$18_{8,10}$	225194.84	149.5	15.7	[2]	...	...
A-HC^{18}OOCH$_3$	$21_{2,20}$-$20_{2,19}$	228083.06	126.5	20.6	228083.6[10]	0.16	0.043
E-HC^{18}OOCH$_3$	$22_{1,22}$-$21_{1,21}$	228865.84	134.4	21.9	[11]	...	0.18
E-HC^{18}OOCH$_3$	$22_{0,22}$-$21_{0,21}$	228866.40	134.4	21.9	[2]	...	...
A-HC^{18}OOCH$_3$	$22_{1,22}$-$21_{1,21}$	228866.72	128.6	21.9	[2]	...	...
A-HC^{18}OOCH$_3$	$22_{0,22}$-$21_{0,21}$	228867.27	128.6	21.9	[2]	...	...
E-HCO^{18}OCH$_3$	$18_{4,14}$-$17_{4,13}$	231398.96	112.9	17.2	231402.3[12]	0.11	0.045
E-HC^{18}OOCH$_3$	$19_{5,14}$-$18_{5,13}$	232102.19	125.3	17.7	232103.0	0.11	0.038
E-HCO^{18}OCH$_3$	$20_{3,18}$-$19_{3,17}$	232673.55	126.1	19.3	232673.9[13]	0.14	0.037
E-HCO^{18}OCH$_3$	$19_{6,14}$-$18_{6,13}$	234214.48	134.5	17.1	234215.5	0.049	0.035
A-HCO^{18}OCH$_3$	$19_{6,14}$-$18_{6,13}$	234226.53	134.4	17.1	234227.5	0.052	0.034
E-HCO^{18}OCH$_3$	$22_{1,22}$-$21_{1,21}$	234336.48	137.7	21.9	234337.6[1]	1.00	0.19
E-HCO^{18}OCH$_3$	$22_{0,22}$-$21_{0,21}$	234336.77	137.7	21.9	[2]	...	...
A-HCO^{18}OCH$_3$	$22_{1,22}$-$21_{1,21}$	234337.43	131.7	21.9	[2]	...	...
A-HCO^{18}OCH$_3$	$22_{0,22}$-$21_{0,21}$	234337.72	131.7	21.9	[2]	...	...
E-HC^{18}OOCH$_3$	$22_{1,21}$-$21_{1,20}$	238283.08	140.9	21.6	238281.4[14]	0.14	0.043
A-HC^{18}OOCH$_3$	$22_{1,21}$-$21_{1,20}$	238288.08	137.9	21.6	238290.1[15]	0.11	0.042
E-HC^{18}OOCH$_3$	$20_{5,16}$-$19_{5,15}$	238745.64	136.1	18.8	238746.7	0.035	0.037
E-HC^{18}OOCH$_3$	$23_{1,23}$-$22_{1,22}$	239045.82	146.3	22.9	239047.3	0.18	0.19
E-HC^{18}OOCH$_3$	$23_{0,23}$-$22_{0,22}$	239046.13	146.3	22.9	[2]	...	...
A-HC^{18}OOCH$_3$	$23_{1,23}$-$22_{1,22}$	239046.64	140.1	22.9	[2]	...	...
A-HC^{18}OOCH$_3$	$23_{0,23}$-$22_{0,22}$	239046.95	140.1	22.9	[2]	...	...
E-HCO^{18}OCH$_3$	$23_{1,23}$-$22_{1,22}$	244760.37	149.9	22.9	244761.5	0.10	0.19
E-HCO^{18}OCH$_3$	$23_{0,23}$-$22_{0,22}$	244760.52	149.9	22.9	[2]	...	...
A-HCO^{18}OCH$_3$	$23_{1,23}$-$22_{1,22}$	244761.26	143.4	22.9	[2]	...	...
A-HCO^{18}OCH$_3$	$23_{0,23}$-$22_{0,22}$	244761.42	143.4	22.9	[2]	...	...
E-HC^{18}OOCH$_3$	$24_{1,24}$-$23_{1,23}$	249224.59	158.7	23.9	[16]	...	0.19
E-HC^{18}OOCH$_3$	$24_{0,24}$-$23_{0,23}$	249224.76	158.7	23.9	[2]	...	...

Table 7. continued.

Species	Transition J_{K_a,K_c}	Rest freq. (MHz)	E_u (K)	S_{ij}	Observed freq. (MHz)	Observed T_{MB} (K)	Modeled T_{MB} (K)
A-HC^{18}OOCH$_3$	$24_{1,24}$-$23_{1,23}$	249225.35	152.1	23.9	[2]	...	...
A-HC^{18}OOCH$_3$	$24_{0,24}$-$23_{0,23}$	249225.52	152.1	23.9	[2]	...	...
E-HCO^{18}OCH$_3$	$24_{1,24}$-$23_{1,23}$	255183.10	162.6	23.9	[17]	...	0.19
E-HCO^{18}OCH$_3$	$24_{0,24}$-$23_{0,23}$	255183.18	162.6	23.9	[2]	...	...
A-HCO^{18}OCH$_3$	$24_{1,24}$-$23_{1,23}$	255183.93	155.7	23.9	[2]	...	...
A-HCO^{18}OCH$_3$	$24_{0,24}$-$23_{0,23}$	255184.02	155.7	23.9	[2]	...	...
E-HC^{18}OOCH$_3$	$24_{2,23}$-$23_{2,22}$	258607.91	166.3	23.6	258607.4	0.094	0.042
A-HC^{18}OOCH$_3$	$24_{2,23}$-$23_{2,22}$	258612.84	162.3	23.6	258612.5[18]	0.13	0.043
E-HCO^{18}OCH$_3$	$21_{7,15}$-$20_{7,14}$	258616.51	166.6	18.5	258617.6	0.094	0.078
E-HC^{18}OOCH$_3$	$24_{1,23}$-$23_{1,22}$	258616.65	166.3	23.6	[2]	...	...
A-HCO^{18}OCH$_3$	$21_{7,15}$-$20_{7,14}$	258619.88	166.6	18.7	258623.5	0.13	0.061
A-HC^{18}OOCH$_3$	$24_{1,23}$-$23_{1,22}$	258621.56	162.2	23.6	[2]	...	...
E-HC^{18}OOCH$_3$	$25_{1,25}$-$24_{1,24}$	259402.10	171.5	24.9	259403.9	0.16	0.19
E-HC^{18}OOCH$_3$	$25_{0,25}$-$24_{0,24}$	259402.19	171.5	24.9	[2]	...	...
A-HC^{18}OOCH$_3$	$25_{1,25}$-$24_{1,24}$	259402.80	164.5	24.9	[2]	...	...
A-HC^{18}OOCH$_3$	$25_{0,25}$-$24_{0,24}$	259402.90	164.5	24.9	[2]	...	...
E-HCO^{18}OCH$_3$	$22_{4,19}$-$21_{4,18}$	262823.90	158.7	21.1	262825.5	0.064	0.039
E-HCO^{18}OCH$_3$	$25_{1,25}$-$24_{1,24}$	265604.62	175.8	24.9	265605.5	0.13	0.19
E-HCO^{18}OCH$_3$	$25_{0,25}$-$24_{0,24}$	265604.66	175.8	24.9	[2]	...	...
A-HCO^{18}OCH$_3$	$25_{1,25}$-$24_{1,24}$	265605.40	168.4	24.9	[2]	...	...
A-HCO^{18}OCH$_3$	$25_{0,25}$-$24_{0,24}$	265605.44	168.4	24.9	[2]	...	...
E-HCO^{18}OCH$_3$	$21_{4,17}$-$20_{4,16}$	267813.37	149.8	20.2	267815.4	0.054	0.042
E-HC^{18}OOCH$_3$	$24_{2,22}$-$23_{2,21}$	268260.21	172.1	23.3	268261.2	0.14	0.041
E-HC^{18}OOCH$_3$	$26_{1,26}$-$25_{1,25}$	269578.30	184.9	25.9	[19]	...	0.21
E-HC^{18}OOCH$_3$	$26_{0,26}$-$25_{0,25}$	269578.35	184.9	25.9	[2]	...	...
A-HC^{18}OOCH$_3$	$26_{1,26}$-$25_{1,25}$	269578.95	177.4	25.9	[2]	...	...
A-HC^{18}OOCH$_3$	$26_{0,26}$-$25_{0,25}$	269579.00	177.4	25.9	[2]	...	...
E-HCO^{18}OCH$_3$	$26_{1,26}$-$25_{1,25}$	276024.88	189.4	25.9	276025.5	0.31	0.19
E-HCO^{18}OCH$_3$	$26_{0,26}$-$25_{0,25}$	276024.90	189.4	25.9	[2]	...	...
A-HCO^{18}OCH$_3$	$26_{1,26}$-$25_{1,25}$	276025.60	181.7	25.9	[2]	...	...
A-HCO^{18}OCH$_3$	$26_{0,26}$-$25_{0,25}$	276025.62	181.7	25.9	[2]	...	...
E-HC^{18}OOCH$_3$	$27_{1,27}$-$26_{1,26}$	279753.14	198.7	26.9	279754.5[20]	0.37	0.18
E-HC^{18}OOCH$_3$	$27_{0,27}$-$26_{0,26}$	279753.16	198.7	26.9	[2]	...	...
A-HC^{18}OOCH$_3$	$27_{1,27}$-$26_{1,26}$	279753.73	190.9	26.9	[2]	...	...
A-HC^{18}OOCH$_3$	$27_{0,27}$-$26_{0,26}$	279753.76	190.9	26.9	[2]	...	...

Notes. Emission lines of ^{18}O-HCOOCH$_3$ present in the frequency range of the 30-m Orion KL survey. Column 1 gives the species; Col. 2: line transition; Col. 3: calculated rest frequencies; Col. 4: energy of the upper level; Col. 5: line strength; Col. 6: observed frequencies; Col. 7: peak line temperature; Col. 8: main-beam temperature obtained with the model. [(1)] Blended with the U-line. [(2)] Blended of several K-components. [(3)] Blended with H^{18}OD. [(4)] Blended with SO^{17}O. [(5)] Blended with SO^{17}O and CH$_3$OCH$_3$. [(6)] Blended with HC$_3$N $\nu_7 = 4$. [(7)] Blended with CH$_3$CH$_2$CN b type. [(8)] Blended with HC$_3$N $\nu_6 = 1^-$. [(9)] Blended with HCOOH. [(10)] Blended with a wing of a CH$_2$CHCN line. [(11)] Blended with HC$_3$N $\nu_7 = 2$. [(12)] Blended with HCOOCH$_3$. [(13)] Blended with ^{13}CH$_3$CCH. [(14)] Blended with H$_2$C^{33}S. [(15)] Blended with a wing of a CH$_2$CHCN $\nu_{11} = 1$ line. [(16)] Blended with CH$_3$CH$_2$CN b type and CH$_2$CHCN $\nu_{15} = 1$. [(17)] Blended with ^{13}CH$_3$OH. [(18)] Blended with CH$_3{}^{13}$CH$_2$CN and DCOOCH$_3$. [(19)] Blended with CH$_3$CH$_2$CN a type. [(20)] Blended with CH$_3$CH$_2{}^{13}$CN.

and LVG codes in that line survey, see Tercero et al. 2010, 2011) as representative parameters for the different cloud components. Our modelling technique also took into account the size of each component and its offset position with respect to IRc2. Corrections for beam dilution were applied to each line depending on their frequency. The only free parameter is therefore the column density. Taking into account the compact nature of most cloud components, the contribution from the error beam is negligible except for the extended ridge, which has a small contribution for all observed lines. In addition to line opacity effects, we discussed other sources of uncertainty in Tercero et al. (2010). Owing to the weakness of the observed lines of ^{18}O-methyl formate, we estimated the uncertainty to be 50% for the column density results.

We assumed a source size of 15″, 10″, 10″, and 120″ of diameter with uniform brightness temperature and optical depth over this size, placed 7″, 7″, 2″, and 0″ from the pointed position for the compact ridge, the "hot" compact ridge, the hot core, and the extended ridge, respectively. The column densities we show are for each state (A, E) of both ^{18}O-methyl formate isotopologues. Column density results were derived for each component obtaining $(4 \pm 2)\times10^{13}$, $(1.5\pm0.7)\times10^{13}$, $(2\pm1)\times10^{13}$, and $(2 \pm 1) \times 10^{13}$ cm^{-2} for the "hot" compact ridge, compact ridge, hot core, and extended ridge, respectively. The total column density derived for each isotopologue is $\simeq(1.0 \pm 0.5) \times 10^{14}$ cm^{-2}. Hence, no isotopic fractionation is found for the two isotopologues ^{18}O of methyl formate. Because methyl formate is mainly emitted from the compact ridge components, we assumed a radial velocity of 7.5 km s^{-1} for the observed frequencies given in Table 7 and Figs. 1 and 2.

Figures 1 and 2 and Table 7 show the comparisons between model and observations. The differences between the intensity of

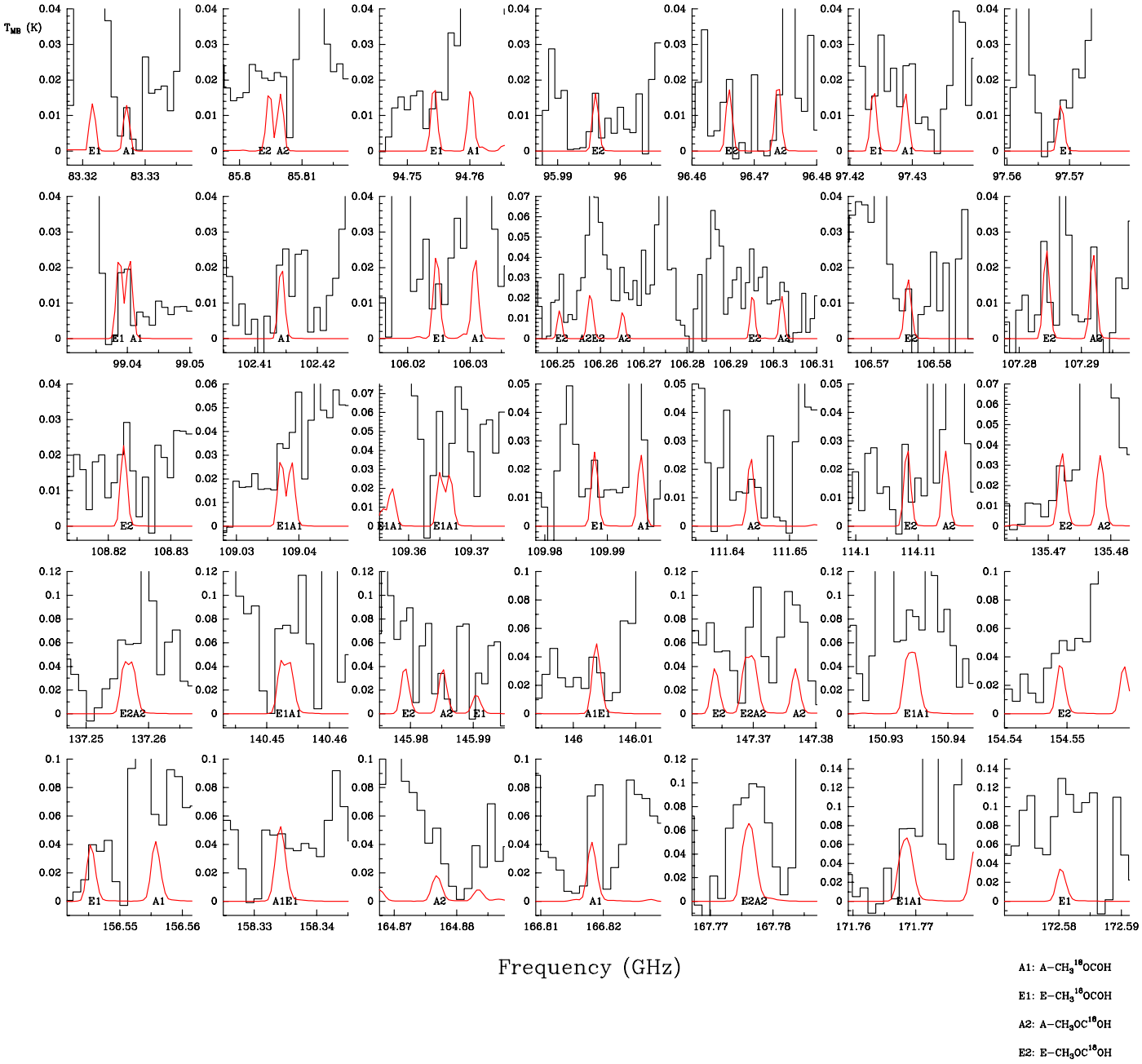

Fig. 1. Observed lines from Orion KL (histogram spectra) and model (thin curves) of ^{18}O methyl formate in the 3 and 2 mm domains. The codes A1, E1, A2, and E2 correspond to A-$CH_3^{18}OCOH$, E-$CH_3^{18}OCOH$, A-$CH_3OC^{18}OH$, and E-$CH_3OC^{18}OH$, respectively. A v_{LSR} of 7.5 km s^{-1} is assumed.

the model and the peak intensity of the observed lines are mostly caused by the contribution of many other molecular species (the frequent overlap with other lines makes it difficult to provide a good baseline for the weak lines of ^{18}O-methyl formate). Nevertheless, the observed line intensity of isolated detected lines of ^{18}O-methyl formate agrees with the model predictions.

The complete modelling of methyl formate including the main isotopologue, the torsionally excited states, and the detected isotopologues, will be published elsewhere (López et al., in prep.).

Together with the results obtained in our previous papers concerning methyl formate (Carvajal et al. 2009; Margulès et al. 2010), we can derive the following ratios for each ^{18}O and ^{13}C methyl formate isotopologues (note that we have obtained the same column density for both isotopologues of each ^{13}C and ^{18}O substitutions of methyl formate): ^{13}C-$HCOOCH_3$/^{18}O-$HCOOCH_3$ $\simeq$ 13 and $HCOOCH_3$/^{18}O-$HCOOCH_3$ $\simeq$ 218 both for the compact ridge component (sum of outer and inner compact ridge). Tercero et al. (2010, 2011) derived $N(O^{13}CS)/N(^{18}OCS)$ = 8 ± 5, $N(^{16}OCS)/N(^{18}OCS)$ = 250 ± 135, and $N(Si^{16}O)/N(Si^{18}O) \gtrsim$ 239, all results agree with the ratios obtained above.

With the emission lines of the ^{18}O methyl formate isotopologues, we conclude the detection of all methyl formate isotopologues that we were able to observe in the line survey of Orion KL of Tercero and coworkers. The 80 lines found correspond to the first detection of ^{18}O-$HCOOCH_3$, together with those of the two ^{13}C isotopologues of methyl formate, and those

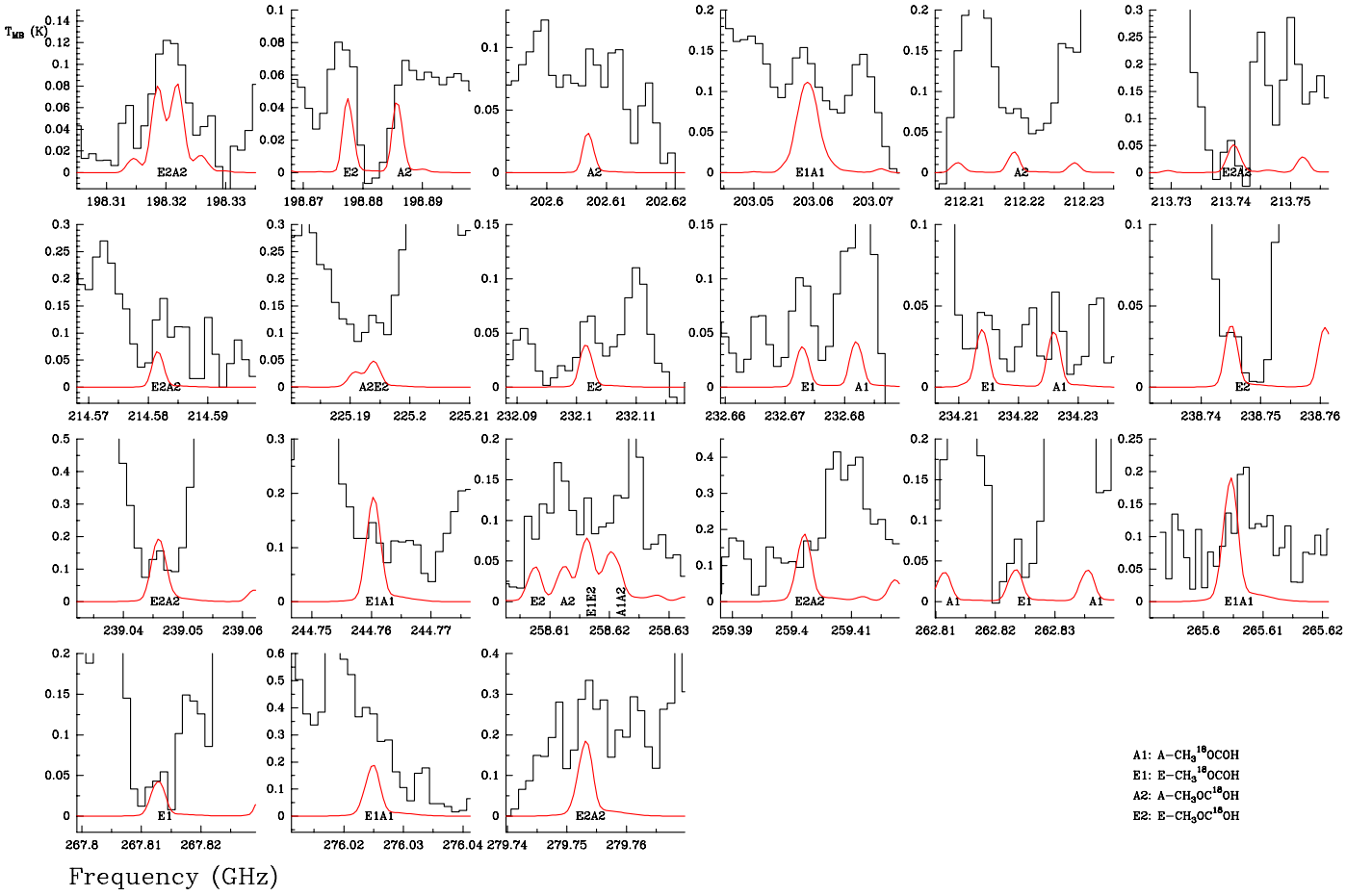

Fig. 2. Observed lines from Orion KL (histogram spectra) and model (thin curves) of ^{18}O methyl formate in the 1.3 mm domain. The codes A1, E1, A2, and E2 correspond to A-CH$_3^{18}$OCOH, E-CH$_3^{18}$OCOH, A-CH$_3$OC^{18}OH, and E-CH$_3$OC^{18}OH, respectively. A $v_{\rm LSR}$ of 7.5 km s^{-1} is assumed.

assigned to the tentative detection of DCOOCH$_3$ (Carvajal et al. 2009; Margulès et al. 2010) contribute with more than 800 lines in the 80-280 GHz domain covered by the Orion line survey of Tercero et al. (2010).

7. Conclusion

We measured and analysed the two ^{18}O isotopic species of methyl formate up to 660 GHz. We treated the internal rotation motion using the rho-axis-method and the BELGI code. We included 4430 and 3258 lines in the fits of 30 and 29 parameters for the ground torsional state for the HCO^{18}OCH$_3$ and HC^{18}OOCH$_3$ species, respectively.

Following these studies, accurate predictions of line positions and intensities were performed. The line survey of Orion KL with the IRAM 30-m telescope permitted the detection of 80 spectral features that correspond to the first detection of the HCO^{18}OCH$_3$ and HC^{18}OOCH$_3$ species.

Acknowledgements. M.C. acknowledges the financial support provided by the Andalusian Government (Spain) project number P07-FQM-03014. He also thanks Université Paris 12 for inviting him. J.C. and B.T. thank Spanish MICINN for support under grants AYA2006-14786, AYA2009-07304 and the CONSOLIDER program "ASTROMOL" CSD2009-00038. This work was supported by the Centre National d'Études Spatiales (CNES) and the Action sur Projets de l'INSU, "Physique et Chimie du Milieu Interstellaire". This work was also done under the ANR-08-BLAN-0054.

References

Blake, G. A., Sutton, E. C., Masson, C. R., & Philips, T. H. 1987, ApJ, 315, 621
Blake, G. A., Mundy, L. G., Carlstrom, J. E., et al. 1996, ApJ, 472, L49
Brown, R. D., Crofts, J. G., Gardner, F. F., et al. 1975, ApJ, 197, L29
Churchwell, E., & Winnewisser, G. 1975, A&A, 45, 229
Carvajal, M., Willaert, F., Demaison, J. & Kleiner, I. 2007, J. Mol. Spectrosc., 246, 158
Carvajal, M., Margulès, L., Tercero, B., et al. 2009, A&A, 500, 1109
Carvajal, M., Kleiner, I., & Demaison. J. 2010, ApJS, 190, 315
Cernicharo, 1985. Internal IRAM report (Granada: IRAM)
Chao, J., Hall, K. R., Marsh, K. N., & Wilhoit, R. C. 1986, J. Phys. Chem. Ref. Data, 15, 1369
Comito, C., Schilke, P., Phillips, T. G., et al. 2005, ApJS, 156, 127
Curl, R.F. 1959, J. Chem. Phys., 30, 1529
Demaison, J., Margulès, L., Kleiner, I., & Császár, A. G. 2010, J. Mol. Spectrosc., 259, 70
Demyk, K., Mäder, H., Tercero, B., et al. 2007, A&A, 466, 255
Demyk, K., Wlodarczak, G., & Carvajal, M. 2008, A&A, 489, 589
Guélin, M., & Thaddeus, P. 1979, ApJ, 227, L139
Herbst, E., Messer, J. K., De Lucia, F. C. & Helminger, P. 1984, J. Mol. Spectrosc., 108, 42
Hougen, J. T., Kleiner, I., & Godefroid, M. 1994, J. Mol. Spectrosc., 163, 559
Ilyushin, V., Alekseev, E. A., Dyubko, S. F., & Kleiner, I. 2003, J. Mol. Spectrosc., 220, 170
Ilyushin, V., Kleiner, I., & Lovas, F. J. 2008, J. Phys. Chem. Ref. Data, 37, 97
Ilyushin, V. V., Kryvda, A., & Alekseev, E. 2009, J. Mol. Spectrosc., 255, 32
Johansson, L. E. B., Andersson, C., Elldér, J., et al. 1984, A&A, 130, 227
Kassi, S., Petitprez, D., & Wlodarczak, G. 2000, J. Mol. Struct., 517, 375
Kirtman, B. 1962, J. Chem. Phys., 37, 2516
Kleiner, I. 2010, J. Mol. Spectrosc., 260, 1
Kobayashi, K., Ogata, K., Tsunekawa, S. & Takano, S. 2007, ApJ, 657, L17

Langer, W. D., & Penzias, A. A. 1990, ApJ, 357, 477
Lees, R. M., & Baker, J. G. 1968, J. Chem. Phys., 48, 5299
Lin, C. C., & Swalen, J. D. 1959, Rev. Mod. Phys., 31, 841
Lovas, F. J. 2004, NIST Recommended rest frequencies for observed interstellar molecular microwave transitions (Gaithersburg, NIST) http://physics.nist.gov/cgi-bin/micro/table5/start.pl
Margulès, L., Coudert, L. H., Møllendal, H., et al. 2009, J. Mol. Spectrosc., 254, 55
Margulès, L., Motiyenko, R., Demyk, K., et al. 2009, A&A, 493, 565
Margulès, L., Huet, T. R., Demaison, J., et al. 2010, ApJ, 714, 1120
Møllendal, H., Leonov, A., & de Meijere, A. 2005, J. Phys. Chem. A, 109, 6344
Møllendal, H., Cole, G. C., & Guillemin, J.-C. 2006, J. Phys. Chem. A, 110, 921
Morino, I., Odashima, H., Matsushima, F., Tsunekawa, S., & Tagaki, K. 1995, ApJ, 442, 907
Morris, M., Palmer, P., & Zuckerman, B. 1980, ApJ, 237, 1
Motiyenko, R. A., Margulès, L., Alekseev, E. A., Guillemin, J.-C., & Demaison, J. 2010, J. Mol. Spectrosc., 264, 94.
Neufeld, D. A., Ashby, M. L. N., Bergin, E. A., et al. 2000, ApJ, 539, L111
Oesterling, L. C., Albert, S., De Lucia, F. C., Sastry, K. V. L. N., & Herbst, E. 1999, ApJ, 521, 255
Pardo, J. R., Cernicharo, J., & Serabyn, E. 2001, IEEE Tras. Antennas and Propagation, 49, 12
Remijan, A., Shiao, Y.-S., Friedel, D. N., Meier, D. S., & Snyder, L.E. 2004, ApJ, 617, 384
Sakai, N., Sakai, T., & Yamamoto, S. 2007, ApJ, 660, 363
Tercero, B., Pardo, J. R., Cernicharo, & Goicoechea, J. R. 2010, A&A, 517, A96
Tercero, B., Vincent, L., Cernicharo, J., Viti, S., & Marcelino, N. 2011, A&A, 528, A26
Willaert, F., Møllendal, H., Alekseev, E., Carvajal, M., Kleiner, I., & Demaison, J. 2006, J. Mol. Struct., 795, 4

Appendix A: Part of the supplementary tables available at the CDS

Table A.1. Assignments, observed frequencies, calculated frequencies from the RAM fit, line strengths, and lower energy levels for ^{18}O-methyl formate ($HCO^{18}OCH_3$) microwave transitions from $v_t = 0$ torsional state included in the fit with parameters of Table 4

	Upper State[a]					Lower State[a]								
num[a]	v_t'	J'	K'_a	K'_c	p'	v''_t	J''	K''_a	K''_c	p''	Obs. Freq. (Unc.)	Calc. Freq (Unc.)	$S(i->f)$	Lower energy
43674	0	52	13	40		0	51	13	39		647718.067(0.050)	647718.144(0.010)	132.312	617.5730
936	0	52	13	40	+	0	51	13	39	+	647719.279(0.050)	647719.183(0.011)	132.309	617.5762
11796	0	58	14	44	+	0	58	12	47	–		647887.350(0.119)	0.930	767.3337
63193	0	58	–14	44		0	58	12	47			647950.687(0.116)	0.931	767.3301
914	0	52	12	41	–	0	51	12	40	–	647997.802(0.050)	647997.830(0.010)	133.472	607.9115
43651	0	52	12	41		0	51	12	40		647998.872(0.050)	647998.826(0.011)	133.473	607.9065
48149	0	60	3	58		0	59	–2	57			648062.209(0.011)	4.994	660.9676
49446	0	60	–2	58		0	59	3	57			648062.209(0.011)	4.994	660.9676
43413	0	60	3	58		0	59	3	57		648062.263(0.050)	648062.209(0.011)	181.830	660.9676
42838	0	60	–2	58		0	59	–2	57		648062.263(0.050)	648062.209(0.011)	181.830	660.9676
683	0	60	3	58	+	0	59	3	57	+	648068.999(0.050)	648068.989(0.011)	181.809	660.9701
91	0	60	2	58	+	0	59	2	57	+	648068.999(0.050)	648068.989(0.011)	181.809	660.9701

Table A.2. Assignments, observed frequencies, calculated frequencies from the RAM fit, line strengths, and lower energy levels for ^{18}O-methyl formate ($HC^{18}OOCH_3$) microwave transitions from vt = 0 torsional state included in the fit with parameters of Table 5

	Upper state[a]					Lower state[a]								
num[a]	v'_t	J'	K'_a	K'_c	p'	v''_t	J''	K''_a	K''_c	p''	Obs. Freq. (Unc.)	Calc. Freq (Unc.)	$S(i->f)$	Lower Energy
81764	0	22	15	7		0	21	14	7		653662.114(0.050)	653662.108(0.005)	7.304	179.8147
81778	0	22	15	8		0	21	14	8		653694.992(0.030)	653695.051(0.006)	7.303	179.8066
71865	0	22	15	8	+	0	21	14	8	–		653703.123(0.004)	6.538	179.8150
71819	0	22	15	7	–	0	21	14	7	+		653703.123(0.004)	6.538	179.8150
1348	0	22	15	8	+	0	21	14	7	+	653703.117(0.030)	653703.123(0.004)	0.763	179.8150
1409	0	22	15	7	–	0	21	14	8	–	653703.117(0.030)	653703.123(0.004)	0.763	179.8150
80449	0	63	–1	62		0	62	–1	61		653877.060(0.050)	653877.075(0.013)	196.986	691.4649
81028	0	63	2	62		0	62	2	61		653877.060(0.050)	653877.075(0.013)	196.986	691.4649
84862	0	63	–1	62		0	62	2	61			653877.075(0.013)	1.888	691.4649
83643	0	63	2	62		0	62	–1	61			653877.075(0.013)	1.888	691.4649
64	0	63	1	62	–	0	62	1	61	–	653881.917(0.030)	653881.876(0.013)	67.659	691.4620
628	0	63	2	62	–	0	62	2	61	–	653881.917(0.030)	653881.876(0.013)	67.659	691.4620

Notes. [a] Upper and lower state quantum numbers are indicated by $'$ and $''$ respectively. Torsion-rotation levels of A species have a "parity" label; levels of E species have a signed Ka value (Herbst et al. 1984). Note that for certain degenerate transitions the sum of line strengths of the degenerate transitions for a given cluster is preserved. [(b)] The first column is a line number, allowing to sort the lines by J and K sub-branches if needed. [(c)] Observed vt = 0 microwave transitions in MHz, with estimated uncertainties in parentheses (in MHz). The data come from Lille-FTMW: 1–19 GHz, Lille-SMM: 150-660 GHz,Oslo: 7-80 GHz. [(d)] Calculated line frequency in MHz with calculated uncertainty in MHz. [(e)] Calculated line strengths in D**2 (for details of the calculation procedure, see text). [(f)] Lower state energy (cm^{-1}) referred to the J = Ka = 0 A-species energy level taken as the zero of the energy (zero-point torsional energy is 66.29250 cm^{-1} for $HC^{18}OOCH_3$ and 66.27348 cm^{-1} for $HCO^{18}OCH_3$).